THE JOURNAL OF PHYSICAL CHEMISTRY B

Article

Cite This: J. Phys. Chem. B 2018, 122, 1747−1755

pubs.acs.org/JPCB

Totally Organic Redox-Active pH-Sensitive Nanoparticles Stabilized by Amphiphilic Aromatic Polyketones

Esteban Araya-Hermosilla,[†] José Catalán-Toledo,[‡] Fabián Muñoz-Suescun,[§] Felipe Oyarzun-Ampuero,[∥] Patrizio Raffa,[†] Lorenzo Massimo Polgar,[†] Francesco Picchioni,[†] and Ignacio Moreno-Villoslada*[,‡]

[†]Department of Chemical Engineering—Product Technology, University of Groningen, Nijenborgh 4, NL-9747 AG Groningen, The Netherlands

[‡]Instituto de Ciencias Químicas, Facultad de Ciencias, Universidad Austral de Chile, Casilla 567, 5090000 Valdivia, Chile

[§]Facultad de Ciencias de la Salud, Universidad Colegio Mayor de Cundinamarca, Bogotá DC, Colombia

[∥]Department of Sciences and Pharmaceutical Technologies, Universidad de Chile, Santiago, Chile

ABSTRACT: Amphiphilic aromatic polymers have been synthesized by grafting aliphatic polyketones with 4-(aminomethyl)benzoic acid at different molar ratios via the Paal−Knorr reaction. The resulting polymers, showing diketone conversion degree of 16%, 37%, 53%, and 69%, have been complexed with the redox-active 2,3,5-triphenyl-2*H*-tetrazolium chloride, a precursor molecule with which aromatic−aromatic interactions are held. Upon addition of ascorbic acid to the complexes, in situ reduction of the tetrazolium salt produced 1,3,5-triphenylformazan nanoparticles stabilized by the amphiphilic polymers. The stabilized nanoparticles display highly negative zeta potential [−(35−70) mV] and hydrodynamic diameters in the submicron range (100−400 nm). Nonaromatic polyelectrolytes or hydrophilic aromatic copolymers showing low linear aromatic density and high linear charge density such as acrylate/maleate and sulfonate/maleate−containing polymers were unable to stabilize formazan nanoparticles synthesized by the same method. The copolymers studied here bear uncharged nonaromatic comonomers (unreacted diketone units) as well as charged aromatic comonomers, which furnish amphiphilia. Thus, the linear aromatic density and the maximum linear charge density have the same value for each copolymer, and the hydrophilic/hydrophobic balance varies with the diketone conversion degree. The amphiphilia of the copolymers allows the stabilization of the nanoparticles, even with the copolymers showing a low linear aromatic density. The method of nanoparticle synthesis constitutes a simple, cheap, and green method for the production of switchable totally organic, redox-active, pH-sensitive nanoparticles that can be reversibly turned into macroprecipitates upon pH changing.

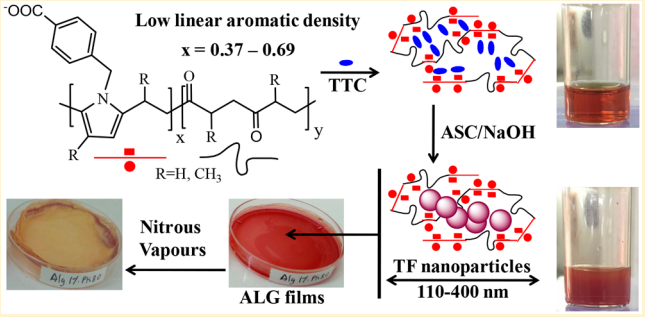

1. INTRODUCTION

Stimuli-responsive materials undergo changes in their chemical, mechanical, or physical properties in response to external triggers,[1−4] such as thermal,[5] electrical,[6] light,[7,8] and chemical[9] stimuli. Devices can be designed by embedding molecules that respond to such external stimuli into polymeric materials.[10,11] In addition, these molecules may be confined and stabilized in responsive nanoparticles.[12−14] The in situ reduction of water-soluble organic molecules in the presence of aromatic polymers is a new, simple, cheap, and green method for the production of total organic redox-active responsive nanoparticles avoiding the use of organic solvents (see Figure 1).[15] Thus, the in situ reduction of the redox-active 2,3,5-triphenyl-2*H*-tetrazolium chloride (TTC) in the presence of an aromatic polyelectrolyte such as poly(sodium 4-styrenesulfonate) (PSS) has been reported to produce nanoparticles of the uncharged 1,3,5-triphenylformazan (TF) stabilized by the aromatic polyelectrolyte.[15] These nanoparticles respond to oxidizing environments by color change. The underlying strategy of this synthesis is that the precursor molecule undergoes short-range aromatic−aromatic interactions with the aromatic polyelectrolyte, releasing water from its hydration sphere, so that the reduction reaction is held in the polymer domain. Performing the redox reaction in the presence of styrenesulfonate/maleate copolymers, showing lower linear aromatic density but higher linear charge density than PSS, did not allow the production of such nanoparticles since the polymers were unable to stabilize them.[15] Here, we hypothesize that the excess of charges over the aromatic groups is responsible for the lack of stabilization ability of these polymers due to their high hydrophilia, so that retention of the precursor molecule in the polymer domain is minimized since the molecules remain hydrated. Thus, for copolymers showing a low linear aromatic density, the confinement of the low-hydrated precursor

Received: November 14, 2017
Revised: January 11, 2018
Published: January 16, 2018

DOI: 10.1021/acs.jpcb.7b11254
J. Phys. Chem. B 2018, 122, 1747−1755

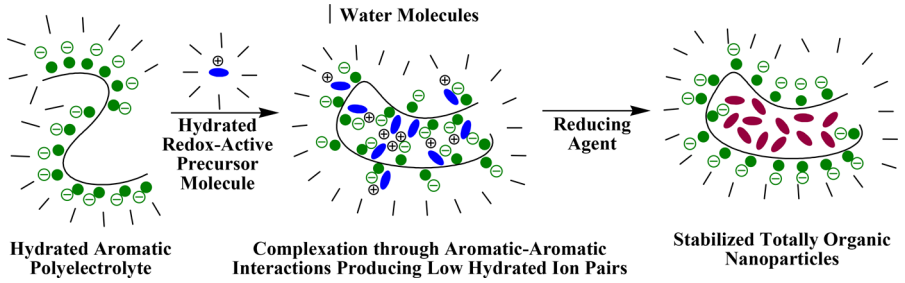

Figure 1. In situ formation of totally organic nanoparticles from redox-active organic molecules able to undergo aromatic−aromatic interactions with aromatic polyelectrolytes.

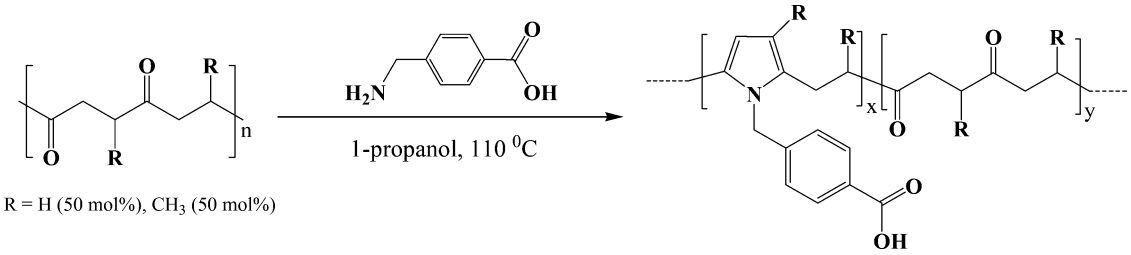

Figure 2. Functionalization of aliphatic polyketones with ABA via the Paal−Knorr reaction.

molecule and stabilization of the resulting particles after redox reaction may be enhanced if the amphiphilia of the polyelectrolyte is increased, so that amphiphilic copolymers bearing uncharged nonaromatic comonomers as spacers between charged aromatic comonomers in the main chain, showing both low linear aromatic density and low linear charge density, may also be used to produce the responsive nanoparticles.

The chemical modification of aliphatic polyketones with primary amines via the Paal−Knorr reaction[16] allows the synthesis of an uncountable number of copolymers with different pendant groups, which may be selected to afford almost any chemical functionality.[17−20] The functionalization reaction is solvent and catalyst free; it can be carried out in one pot, and it yields water as its only byproduct. The reaction converts 1,4-diketone groups in pyrrole groups. Thus, the resulting copolymers show a hydrophobic backbone composed of unreacted ketones and substituted pyrroles; by choosing charged or polar pendant groups in the pyrrole substituents, amphiphilic polymers with different copolymer composition may be produced showing different hydrophobic/hydrophilic balance.

In this paper, the synthesis of amphiphilic copolymers showing different linear aromatic and charge density will be shown, based on the Paal−Knorr reaction of aliphatic polyketones with different amounts of 4-(aminomethyl)benzoic acid (ABA). The ability of the different copolymers to undergo aromatic−aromatic interaction with the redox-active precursor molecule TTC will be explored by ^{1}H NMR. In situ reduction of the precursor molecule in the presence of the different copolymers will be held with the aid of ascorbic acid (ASC), and the formation of totally organic nanoparticles of TF stabilized by the different amphiphilic polyelectrolytes will be evaluated. In addition, due to the weak-acid nature of the benzoic residue, the sensitivity to the pH of the formed nanoparticles will be studied.

2. EXPERIMENTAL SECTION

2.1. Materials. Aliphatic polyketones made of ethylene, propylene, and carbon monoxide were synthesized according to a reported procedure,[21,22] yielding a polyketone with hydrocarbon segments composed of 50 mol % ethylene and 50 mol % propylene (PK50, MW 3636 g/mol). Sodium alginate (ALG, Buchi, MW 198 g/mol of monomeric units), glycerol (Sigma-Aldrich, MW 92 g/mol), 4-(aminomethyl) benzoic acid (ABA) (Sigma-Aldrich, MW 151.16 g/mol, 97%), 2,5-hexanedione (Sigma-Aldrich, MW 114.14 g/mol, 98%), 2,3,5-triphenyl-2*H*-tetrazolium chloride (TTC) (Merck, MW 334.80 g/mol, 95%), 1-propanol (Sigma-Aldrich), dimethyl sulfoxide-d_6 (Sigma-Aldrich), HNO_3 (Caledon 16.64 M), HCl (Sigma-Aldrich), and NaOH (Merck) were used as received. Milli-Q water was used to prepare the different solutions.

2.2. Equipment. ^{1}H NMR spectra were recorded using a Varian Mercury Plus 400 MHz spectrometer. ATR FT-IR measurements were done in a Thermo Nicolet NEXUS 670 FT-IR. Elemental analyses were done in a Euro EA elemental analyzer. The pH was controlled with a pH-meter, Seven2Go. Scanning transmission electron microscopy (STEM) analyses were done in an Inspect 50 microscope (FEI). Dynamic light scattering (DLS) measurements were done in a Nano ZS zetasizer equipment (Malvern) with backscatter detection (173°), controlled by the Dispersion Technology Software (DTS 6.2, Malvern). UV−vis spectra were recorded in a Jasco 750 spectrometer. ALG films were prepared in a Wise Cube (Wisd) incubator.

2.3. Methods. *Model Compound.* 2,5-Hexanedione was used as a model system to allow for a precise assignment of ^{1}H NMR signals after the Paal−Knorr reaction with ABA. The reaction between stoichiometric amounts of ABA and 2,5-hexanedione was performed in a 100 mL round-bottom flask equipped with a magnetic stirrer, a reflux condenser, and an oil bath. First, 2.05 g of 2,5-hexanedione (0.018 mol) and 2.72 g of ABA (0.018 mol) were dissolved in 1-propanol (30 mL). Although the Paal−Knorr reaction may be performed in general without the use of any solvent, in this work the

DOI: 10.1021/acs.jpcb.7b11254
J. Phys. Chem. B 2018, 122, 1747−1755

Table 1. PK50 and ABA Feed Ratios and the Corresponding *x*

polyketone derivative (PK50ABA*x*)	PK50 (g)	moles of dicarbonyl group	ABA (g)	moles of ABA	*N* (%)	*x*	M_+ (g/mol of basic groups)
PK50ABA16	19.49	0.15	4.68	0.031	1.52	0.16	903
PK50ABA37	19.52	0.15	9.37	0.062	3.10	0.37	456
PK50ABA53	19.73	0.16	14.20	0.093	3.98	0.53	353
PK50ABA69	19.10	0.15	18.33	0.12	4.54	0.69	298

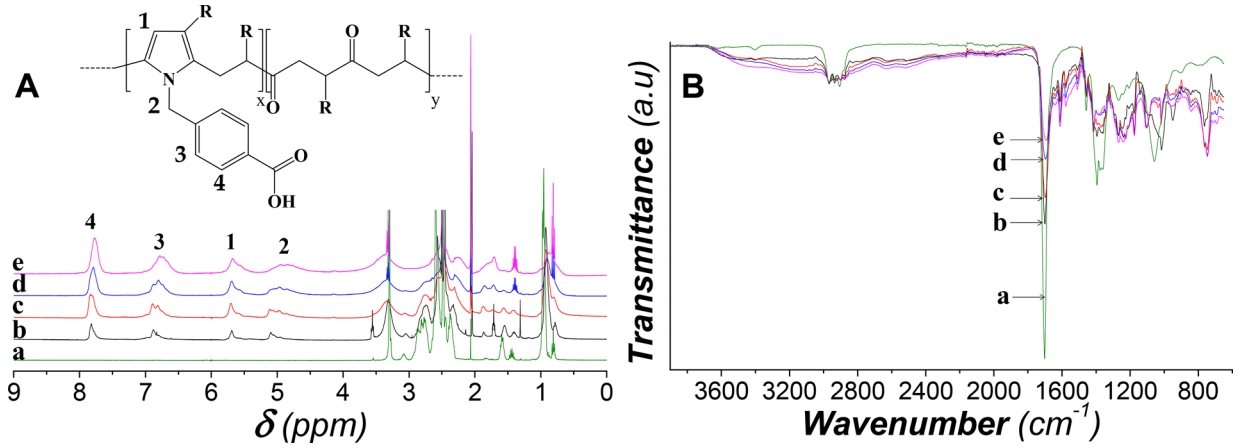

Figure 3. ^{1}H NMR (A) and ATR FT-IR (B) spectra of PK50ABA*x* at *x* values of 0.0 (a), 0.16 (b), 0.37 (c), 0.53 (d), and 0.69 (e).

functionalization was carried using 1-propanol because the primary amine was obtained as a powder. The reaction was carried out at 100 °C under stirring (700 rpm) for 24 h. The sample was then placed in a 50 °C oven for 48 h to evaporate the solvent. ^{1}H NMR spectra were recorded using dimethyl sulfoxide-d_6 as solvent: δ = 2.2 ppm (s, 6 H, CH_3), 5.1 ppm (s, 2H, CH_2), 5.8 ppm (s, 2H, =CH—CH=), 6.96 ppm (d, 2H, benzoic-H), 7.89 (d, 2H, benzoic-H).

Polyketone Modification. The functionalization of PK50 with ABA (see Figure 2) was carried out at different 1,4-dicarbonyl/primary amine molar ratios (see Table 1). Around 20 g of PK50 and the appropriate amount of ABA was dissolved in 1-propanol in a 100 mL round-bottom flask equipped with magnetic stirrer, reflux condenser, and an oil bath. The reaction was carried out at 100 °C under stirring (700 rpm) for 24 h. The solvent was then evaporated in a vacuum oven at 50 °C for 48 h. The dried polymers were ground and washed three times with deionized Milli-Q water to remove any unreacted ABA. The remaining water was removed by freeze-drying for 48 h. The resulting polymers were characterized by ATR FT-IR and ^{1}H NMR using dimethyl sulfoxide-d_6 as solvent. The carbonyl conversion (*x*) is defined as the molar fraction of 1,4-dicarbonyl units converted via the Paal–Knorr reaction, and, on the basis of elemental analysis, is calculated following eq 1.[19]

$$x = \frac{NM_c}{nM_N + N(M_c - M_p)} \quad (1)$$

Here *N* is the nitrogen content (in g) per g of polymer, M_N the atomic mass of nitrogen (14 g/mol), *n* the number of nitrogen atoms present in the converted 1,4-dicarbonyl segment (1 in this case), M_p the molecular weight of the converted 1,4-dicarbonyl segment (241 g/mol in this case), and M_c the molecular weight of the nonconverted 1,4-dicarbonyl segment (126 g/mol in this case). M_p and M_c were calculated taking into account the presence of ethylene and propylene in the original polyketone copolymer PK50 at a 1:1 ratio. In order to adjust the stoichiometry of charged groups when using the polyketone derivatives, we consider a polymeric molecular weight given in g/mol of basic groups (M_+, see Table 1) following eq 2:[19]

$$M_+ = \frac{xM_p + yM_c}{xz} \quad (2)$$

where *y* is the fraction of nonconverted 1,4-dicarbonyl groups, provided that $x + y = 1$, and *z* is the number of atoms susceptible to protonate in the converted repetitive unit, in this case 1, provided that the dicarbonyl moieties are not susceptible to protonation.

Nanoparticle Preparation. Stock aqueous solutions of PK50ABA37, -53, and -69 (0.1 M), and TTC (0.1 M) were carried to pH 12 using minimum amounts of NaOH (1 M). A stock solution of ASC at 1.2×10^{-2} M was also prepared. Definite amounts of water, TTC, and polymer stock solutions were mixed until the desired molar concentrations were reached. Then, a small excess of ASC over TTC (1.2-fold in mol) was added to the mixture, together with NaOH to ensure pH 12. Particular conditions are given in the figure captions. STEM images were obtained by sticking a droplet (10 μL) of the nanoparticle suspension on a copper grid (200 mesh, covered with Formvar) for 2 min, then removing the droplet with filter paper avoiding the paper touching the grid, then washing twice the grid with a droplet of Milli-Q water for 1 min, and removing the droplet with filter paper. Later, the sample was stained with a solution of 1% phosphotungstic acid by sticking a droplet of this solution on the grid for 2 min and removing the droplet with filter paper. Finally, the grid was allowed to dry for at least 1 h before analysis. The hydrodynamic diameter and zeta potential of the resulting TF nanoparticles were analyzed by DLS at 25 °C. Results are considered valid under the criteria of the DTS 6.2 software (Malvern); correlograms of suspensions showing invalid results of size may also be discussed.

ALG Film Preparation. A stock aqueous solution containing 2% ALG and 1% glycerol was mixed at a 1:1 volume ratio with an aqueous solution containing TF/PK50ABA*x* nanoparticles

DOI: 10.1021/acs.jpcb.7b11254
J. Phys. Chem. B 2018, 122, 1747–1755

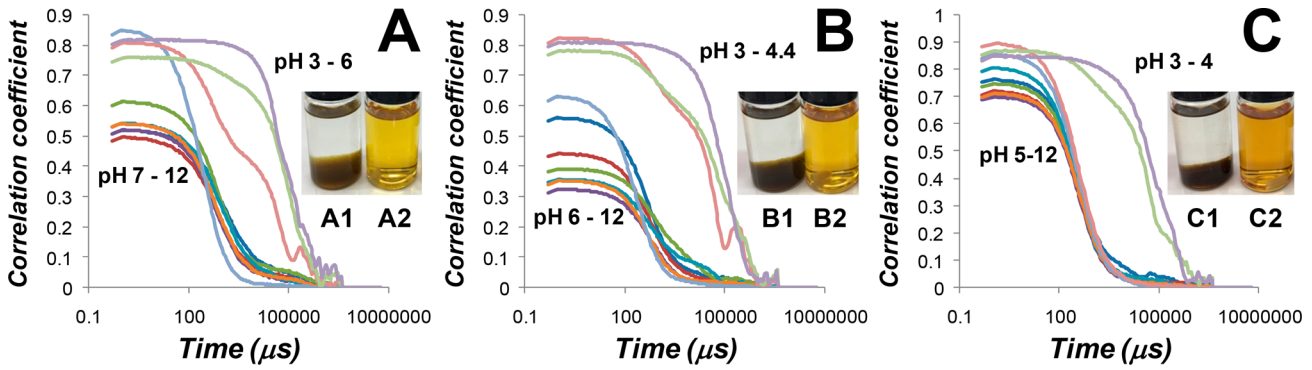

Figure 4. Optical images of 10^{-3} M of PK50ABA*x* at acid (1) and basic (2) pH, and correlograms obtained upon titration of the corresponding basic solutions with HCl, for *x* values of 0.37 (A), 0.53 (B), and 0.69 (C).

obtained after reduction, with 1.2×10^{-3} M of ASC, of a mixture of TTC at 1.0×10^{-3} M and PK50ABA*x* at a concentration of 2×10^{-3} M. Then, 3 mL portions of the resulting suspensions were poured into plastic plates of 2.5 cm of diameter, and left to dry in the incubator for 18 h at 37 °C and 30 rpm. Once the transparent films were formed, they were characterized by absorption UV−vis spectroscopy using a clean plastic plate as background. Discoloration of the films was assayed with nitrous vapors in a laboratory fume hood. A 20 mL portion of concentrated HNO_3 was placed in a 100 mL flask. The flask was covered with Parafilm M, and holes were practiced with a needle. The ALG films were subsequently detached from the plastic plates, and placed on top of the Parafilm-covered 100 mL flask. Then, Cu^0 plates of 260 mg were carefully dripped into the HNO_3 solution, and the whole system was immediately covered with an inverted 1 L flask. The films were exposed to the nitrous vapors for 15 min, and then left to aerate for 30 min before analysis by UV−vis.

3. RESULTS AND DISCUSSION

3.1. Polyketone Modification. After polymer synthesis and purification, the products were analyzed by elemental analysis in order to calculate *x*. The result can be seen in Table 1. It can be seen that the conversion was not quantitative concerning the stoichiometry of the primary amine included in the feed, especially for the highest *x* intended. Thus, at molar ratios in the feed of 80, 60, 40, and 20%, the values of *x* achieved were 0.69, 0.53, 0.37, and 0.16, respectively, values that are included in the respective code names of the polymers (PK50ABA*x*). The successful functionalization of PK50 with ABA was confirmed by ATR FT-IR and ^{1}H NMR spectroscopies. The broad peaks observed in NMR spectra are a result of the polymeric nature of the molecules together with the statistical distribution of ethylene and propylene (Figure 3A).[23] The assignment of the signals can be contrasted with that of the model compound NMR signals described in the Experimental Section. The polymers display a pyrrole ring whose protons appear between 5.5 and 6.0 ppm (proton 1). Methylene protons found between the pyrrole ring and the benzoic group (proton 2) can be found at around 5 ppm. Finally, the signals at 6.7 and 7.7 ppm are assigned to protons of the benzoic group (protons 3 and 4). On the other hand, the ATR FT-IR spectra of the polymers can be seen in Figure 3B. The intensity of the IR signal of the carbonyl stretching ($\nu_{CO} \approx 1700$ cm^{-1}) decreases when the 1,4-dicarbonyl moieties are converted into pyrrole rings via the Paal−Knorr reaction,[24] corresponding to the disappearance of two ketone carbonyls and appearance of one carboxylate carbonyl. The intensity of the scissoring bending vibration of the CH_2 next to the carbonyl group and the symmetrical bending vibration of the CH_3 (1399−1350 cm^{-1}) decreases with *x*. Simultaneously, a weak broad peak corresponding to the hydrogen bonding between the carboxylic groups (3700−2000 cm^{-1}), two peaks corresponding to the asymmetrical and symmetrical stretching of C—H (2969 and 2873 cm^{-1}, respectively), a series of weak peaks corresponding to the C═N and C═C stretching of the pyrrole ring and benzoic group (1650−1500 cm^{-1}), and the peak corresponding to the out-of-plane C—H bending of the benzoic group (745 cm^{-1}) increasingly appear upon increasing *x*.

Finally, the solubility in water of the different copolymers was analyzed. PK50ABA16 was not soluble in water, due to the low content of hydrophilic groups. Since the benzoic group is a weak acid, the polymers are pH-responsive, so that PK50ABA37, PK50ABA53, and PK50ABA69 are insoluble in water at acidic pH, but soluble, or at least dispersible, at basic pH, as shown in Figure 4. The transition between the two macroscopic phases is analyzed by DLS. Although the correlograms do not show accurate apparent particle size, there is an evident change in them upon macroprecipitation, that allows identification of the transition between both phases at pH falling in the range 6−7 for PK50ABA37, 4.4−6 for PK50ABA53, and 4−5 for PK50ABA69, as can be also seen in Figure 4, showing a shift to lower values as the linear charge density increases.

3.2. Aromatic−Aromatic Interactions between PK50ABA*x* and TTC. The three water-soluble amphiphilic aromatic polyketones obtained at different *x* (PK50ABA37, -53, and -69), and thus showing a respective increase on the linear aromatic density, were mixed with 10-fold less concentrated TTC, and the mixtures were analyzed by ^{1}H NMR to corroborate the occurrence of short-range aromatic−aromatic interactions in D_2O. The 1D spectra are shown in Figure 5. Peaks corresponding to TTC protons were assigned according to a previous work,[25] as can be seen in Figure 5A. In the presence of the aromatic polyketones, TTC signals undergo peak broadening, related with a decrease in molecular mobility, and upfield shifting, as a consequence of a different chemical environment produced by the proximity of other aromatic rings that produce magnetic fields associated with their aromatic electron currents.[25−28] As *x* increases, and thus the linear aromatic density, the shifting of the signals also increases; for instance, the signal corresponding to TTC proton 1 shifts from 8.4 to 8.04, 7.97, and 7.93 ppm in the presence of PK50ABA37, -53, and -69, respectively. In the case of the aromatic proton

DOI: 10.1021/acs.jpcb.7b11254
J. Phys. Chem. B 2018, 122, 1747−1755

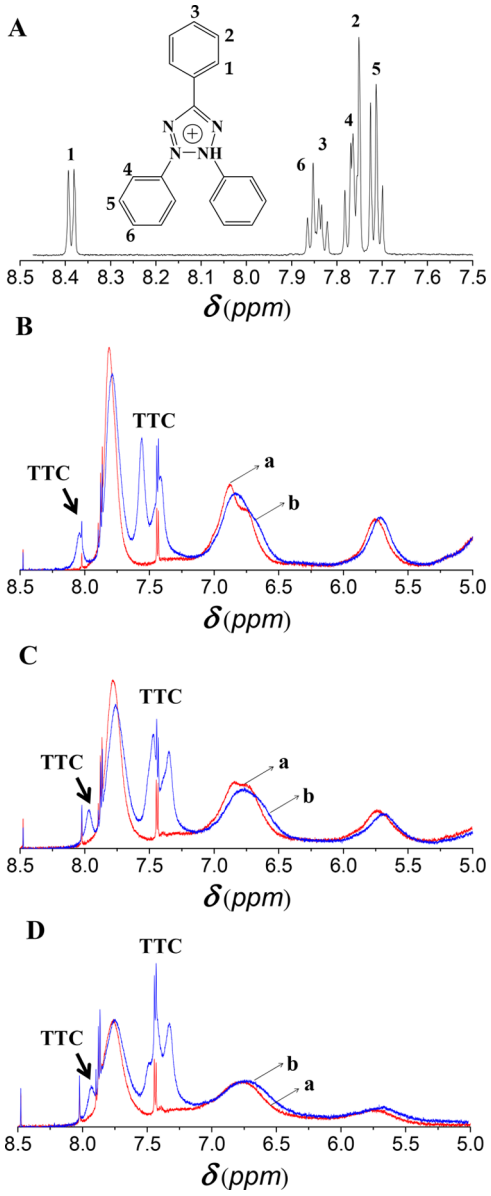

Figure 5. ^{1}H NMR spectra in D_2O of TTC 10^{-3} M (A), PK50ABA*x* 10^{-2} M (a), and their corresponding mixtures (b), at *x* values of 0.37 (B), 0.53 (C), and 0.69 (D).

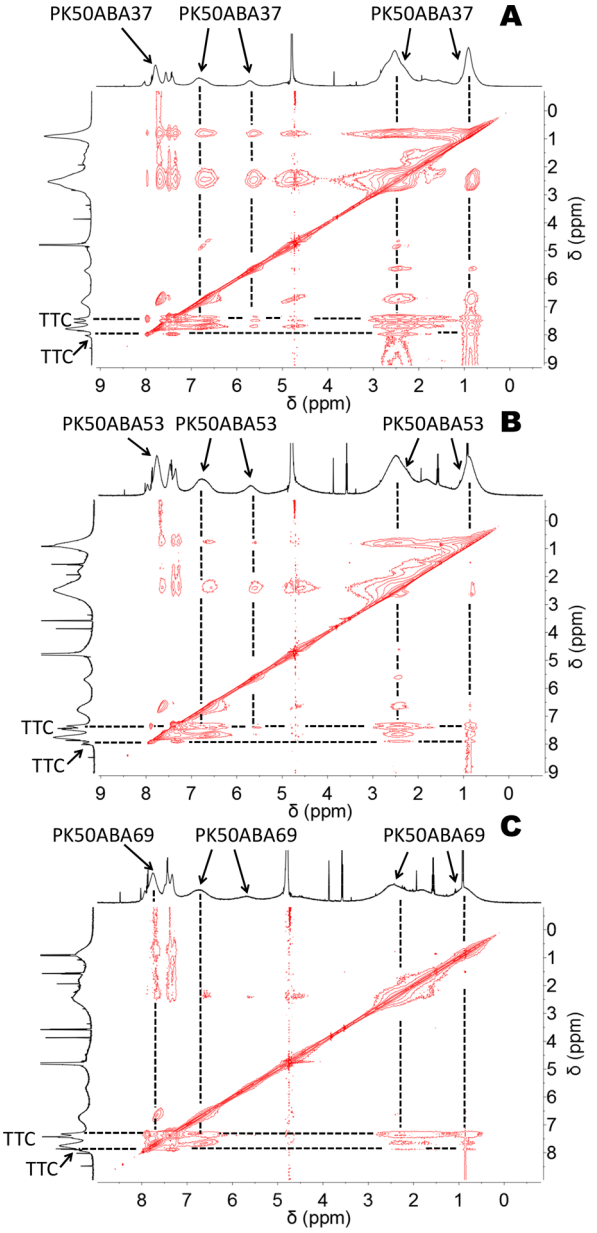

Figure 6. 600 MHz NOESY spectra in D_2O of 10^{-3} M of TTC in the presence of 10^{-2} M of PK50ABA37 (A), PK50ABA53 (B), and PK50ABA69 (C).

signals of the polymers, upfield shifting in the range 0.01−0.04 ppm is also found (Figure 5B−D).

Definite evidence of the occurrence of short-range aromatic−aromatic interactions between TTC and the copolymers, which implies the release of water from the hydration shell of the aromatic rings, thus undergoing intimate contact, may be provided by 2D NOESY experiments. The results can be seen in Figure 6. Cross-peaks appear between signals of TTC and the copolymers, independent of their *x*, indicating magnetization transfer across the space, a condition for which the molecules should keep a mutual distance lower than 5 Å.

3.3. TF Nanoparticles Stabilized by the PK50ABA*x*. Reduction of 10^{-3} M of TTC with ASC in the presence of 10^{-2} M of PSS allows the formation of total organic nanoparticles of TF stabilized by the aromatic polymer, but in the presence of 10^{-2} M of the corresponding alternating copolymer with maleate the nanoparticles could not be stabilized.[15] In order to establish comparisons, we perform here reduction reactions at the same conditions and concentration of the precursor molecule and the amphiphilic aromatic copolymers PK50ABA*x*, i.e., at 10^{-2} M of the copolymer aromatic groups, and 10-fold less concentrated TTC. As in the case when the concentration is 10^{-3} M, at the concentration of 10^{-2} M the pristine polymers formed clear solutions. However, it can be seen in Figure 7 that the reduction of TTC produced the formation of suspended TF particles stabilized by all three copolymers, independent of the value of *x*, witnessed by the opalescent appearance of the suspensions, and corroborated by STEM and DLS analyses whose results are shown, respectively, in Figures 8 and 9. This confirms our hypothesis, so that the amphiphilia of the polyelectrolyte enhances the stabilization of the particles, so that amphiphilic polymers showing low linear aromatic density and low linear charge density may also be used to produce responsive nanoparticles.

DOI: 10.1021/acs.jpcb.7b11254
J. Phys. Chem. B 2018, 122, 1747−1755

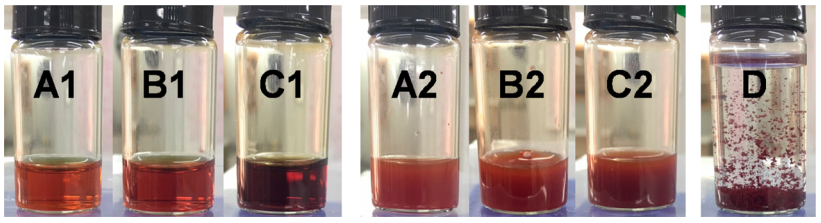

Figure 7. Optical images of samples containing 10^{-2} M of PK50ABA37 (A), PK50ABA53 (B), and PK50ABA69 (C), in the presence of 10^{-3} M of TTC (1) and in the presence of TF (2) after reduction of 10^{-3} M of TTC with ASC. (D) TF precipitates after reduction of 10^{-3} M of TTC with ASC.

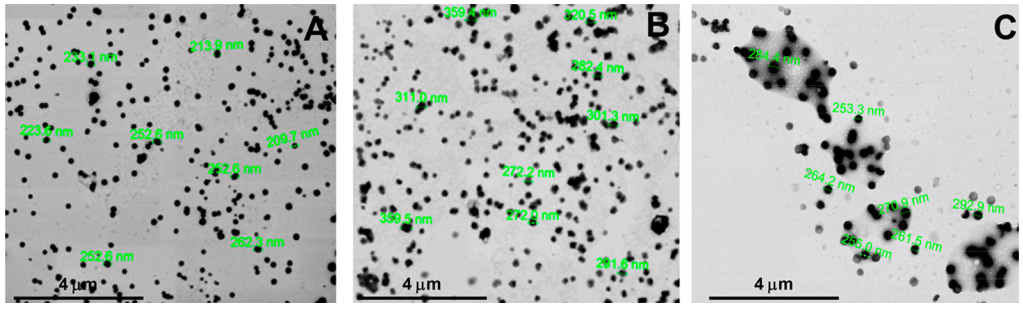

Figure 8. STEM images of deposits on copper grids of suspensions of stabilized TF nanoparticles obtained after reduction of 10^{-3} M of TTC with ASC in the presence of 10^{-2} M of PK50ABA37 (A), PK50ABA53 (B), and PK50ABA69 (C).

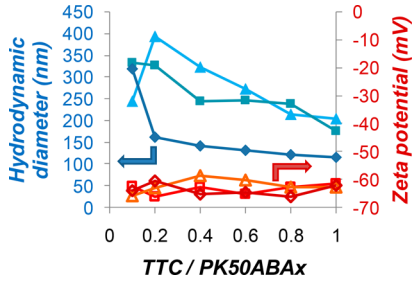

Figure 9. Apparent size (filled symbols) and zeta potential (empty symbols) of TF nanoparticle samples containing 10^{-2} M of PK50ABA37 (▲, △), PK50ABA53 (■, □), and PK50ABA69 (♦, ◇), obtained after reduction of variable amounts of TTC with ASC.

STEM results show (Figure 8), after deposition of the suspensions in copper grids, nanoparticles of size of the same order of magnitude of that shown by DLS in Figure 9, indicating that the nanoparticles are probably solid nanoprecipitates.

Monodisperse distributions of TF nanoparticles stabilized by the polymers are found not only at these conditions, but also at increasing concentrations of the precursor molecule TTC, at least in the range of TTC/polymer of 0.1−1.0, as can be seen in Figure 9. The size of the particles ranged between 110 and 400 nm, being higher at lower TTC/polymer ratio. The PDI values ranged between 0.06 and 0.21, showing a narrow distribution of particle size, as can be also inferred after analysis of the STEM images shown in Figure 8. The zeta potential stayed at absolute

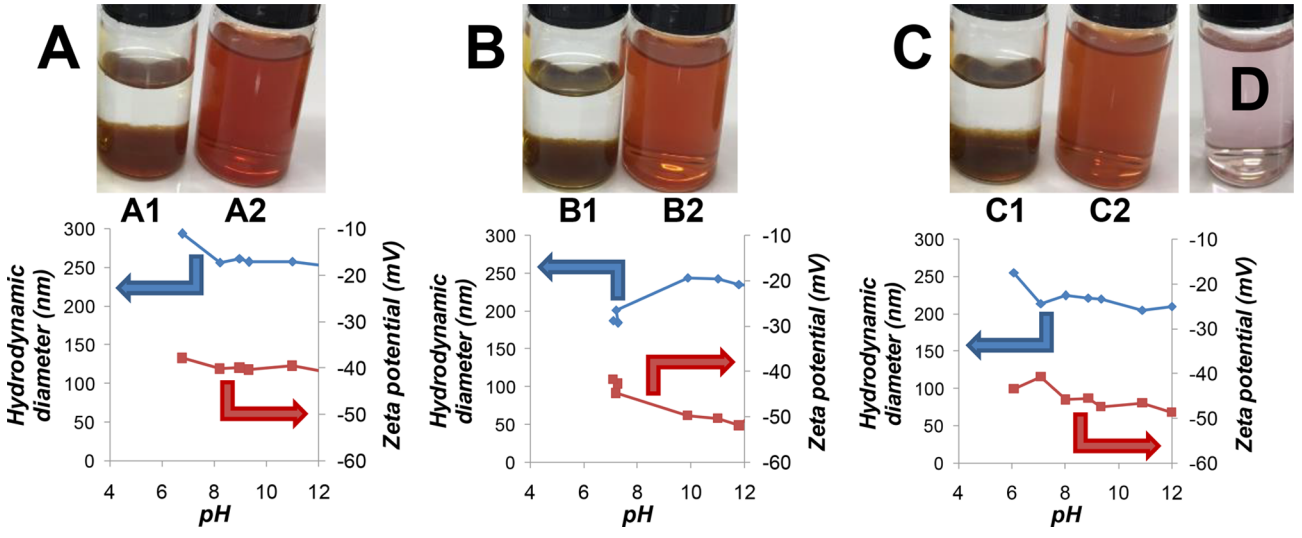

Figure 10. Optical images after reduction of 5×10^{-4} M of TTC with ASC in the presence of 10^{-3} M of PK50ABA37 (A), PK50ABA53 (B), and PK50ABA69 (C) at acid (1) and basic (2) pH, and apparent size (♦) and zeta potential (■) of the resulting TF/polymer suspensions upon titration as a function of pH. TF in water after reduction of 5×10^{-4} M of TTC with ASC (D).

DOI: 10.1021/acs.jpcb.7b11254
J. Phys. Chem. B 2018, 122, 1747−1755

values high enough to ensure stability of the particles in time, at least for 7 days.

When the concentration of the precursor TTC takes values of 5×10^{-4} M or less, the reduction product TF becomes soluble (or at least dispersible), as can be seen in Figure 10D. Titration of the corresponding nanoparticles stabilized at basic pH by the different polymers at a concentration of 10^{-3} M, comparable to titrations shown in Figure 4, showed that the precipitation of the polymers at acidic pH involves coprecipitation of the TF molecules (see Figure 10A–C), since the supernatant does not show the characteristic red color of TF. At pH over the transition pH between the suspended and the precipitate phases, nanoparticles of apparent size ranging between 170 and 300 nm were found, showing PDI values ranging between 0.18 and 0.44, and the corresponding negative zeta potential achieved absolute values higher than 35 mV, which allows the nanoparticles to be stable for at least 7 days.

The phase transition shown in Figure 10 witnesses that the formulations, which involve both PK50ABA*x* and TF are pH-sensitive. Interestingly, once the material precipitated at low pH, increasing the pH to values higher than the transition pH allows the stabilized TF nanoparticles to be reconstituted. This can be done at least for 6 cycles. Our experimental results show that, taking into account the three systems and 6 cycles, the apparent size of the reconstituted nanoparticles ranged between 156 and 246 nm, with PDI ranging between 0.12 and 0.41, and zeta potential ranging between −26 and −40 mV.

3.4. Final Remarks. Aromatic–aromatic interactions are common in nature and synthetic systems[29−32] and play a pivotal role in the stability of the DNA double helical structure,[33,34] molecular recognition,[35] and protein structure and functionality.[36,37] Aromatic–aromatic interactions in water are reinforced by the hydrophobic effect, with both an enthalpic and an entropic contribution to the free energy by water released from the hydration spheres of the aromatic solutes.[38] In addition, long-range electrostatic interactions do also contribute to the complexation between polyelectrolytes bearing charged aromatic groups and complementary charged aromatic low-molecular-weight molecules by aromatic–aromatic interactions.[15,25,27,28,39−41] Once both species approach each other, and water molecules from the respective hydration spheres are released, site-specific short-range interactions, such as π-stacking, cation–π interaction, hydrogen bonding, or short-range electrostatic interactions, contribute to the strong binding with a preferential geometry. If ion pairs are formed between the complementary charged aromatic moieties, these ion pairs may be stabilized in hydrophobic environments furnished by their self-aggregation, as clearly shown for the interaction between the aromatic polyelectrolyte PSS and xanthene dyes.[28,41−45]

In this context, copolymerization of charged aromatic monomers with charged nonaromatic ones gives rise to highly charged polymers bearing tunable linear aromatic density. The behavior of these copolymers is intermediate between aromatic polyelectrolytes and nonaromatic ones. Indeed, the nonaromatic charged segments furnish hydrophilia and rigidity to the polymer chain, so that the stabilization of ion pairs formed between the aromatic comonomers and aromatic counterions in hydrophobic environments is jeopardized. This has been observed for copolymers of PSS and maleic acid showing different linear charge and aromatic density upon interaction with several molecules,[15,26,40,44,45] including TTC.[26,40] As a consequence of this, TF nanoparticles synthesized by the same method used here could only be stabilized by the polymers PSS and poly(sodium 4-styrenesulfonate-*co*-maleic acid) at a comonomer composition 3:1 [P(SS_3-*co*-MA_1)], but not in the presence of the corresponding copolymer at a comonomer composition 1:1 [P(SS_1-*alt*-MA_1)], or the comparable nonaromatic polyelectrolyte poly(acrylic acid-*alt*-maleic acid) [P(AA_1-*alt*-MA_1)].[15]

In this work we can see, however, that increasing the hydrophobia of the polyelectrolytes, it is possible to produce TF nanoparticles stabilized by the copolymers showing a low linear aromatic density. The PK50ABA*x* copolymers show nonaromatic comonomers which are uncharged. In addition, since the charged aromatic moieties are relatively far from the backbone, and linked to aromatic pyrrole groups in the backbone through a methylene spacer, a hydrophobic environment is easily furnished to ion pairs formed with the aromatic precursor molecule, which further will stabilize the TF resulting nanoparticles upon reduction with ASC.

Applications of these nanoparticles may stand on the redox properties of the TTC/TF couple, accompanied by color change, as have been used at a molecular level for the detection of bacteria,[46] to quantify reducing carbonyl groups in cellulose,[47] to determine mammalian cell growth,[48] and to sense metal ions.[49] The stabilized TF nanoparticles may be easily incorporated in devices and matrices from aqueous suspensions, as for example in hydrogels.[15] Another proof of concept is shown here. The TF/PK50ABA*x* nanoparticles were included in ALG films containing glycerol. As can be seen in Figure 11A, acceptable homogeneity is afforded upon suspension of the stabilized TF nanoparticles in ALG solutions and subsequent solvent evaporation. The red color of the films could be checked by absorption UV–vis measurements finding a wide band at around 500 nm, as can be seen in Figure 11B. After exposure of the films to nitrous vapors, oxidation of TF occurs, and the red color of the films disappears, noticed both at naked eye and by the disappearance of the band centered at around 500 nm. This property may promote these colorimetric responsive materials to be used as flow sensors and protection materials where there is risk of the presence of oxidizing vapors, such as in fractured or corroded pipelines, leaking joints, flow chambers, fume hoods, etc. In addition, the TF/PK50ABA*x* nanoparticles are sensitive to the pH, so that macroprecipitates are formed under a definite pH between 4 and 6, which slightly varies with the value of *x*. This property could be also used to produce pH-responsive materials and devices. The functional-

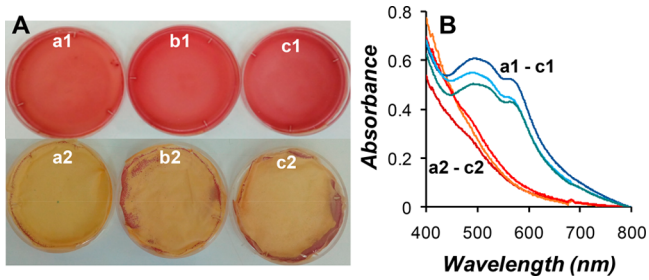

Figure 11. (A) Optical images of ALG films containing TF nanoparticles stabilized with PK50ABA37 (a1, a2), PK50ABA53 (b1, b2), and PK50ABA69 (c1, c2), before (a1, b1, c1) and after (a2, b2, c2) discoloration with nitrous vapors. (B) Corresponding UV–vis spectra.

DOI: 10.1021/acs.jpcb.7b11254
J. Phys. Chem. B 2018, 122, 1747−1755

ization of polyketones with primary amines by the Paal−Knorr reaction can be considered a clean technology since no solvent is needed and it affords water as the only byproduct of the reaction. The synthesis of the PK50ABA*x*/TTC complexes, and the reduction reaction to afford the TF nanoparticles, occurs in water, without the need of any organic solvent. This technology contributes, thus, to the fabrication of responsive materials under the precepts of the green chemistry.

4. CONCLUSIONS

The production of redox-active, pH-sensitive, totally organic stimuli-responsive nanoparticles via a simple, cheap, and green method was accomplished utilizing the aromatic redox-active precursor molecule TTC and the amphiphilic aromatic pH-sensitive copolymers PK50ABA*x*. Water-soluble PK50ABA*x* materials showing values of *x* of 69, 53, and 37 were successfully synthesized by the chemical modification of the aliphatic polyketone PK50 with 80%, 60%, and 40% molar ratio in the feed of ABA, respectively, via the Paal−Knorr reaction. Complexation of TTC with the amphiphilic copolymers involves aromatic−aromatic interactions, as seen by 1D and 2D NOESY ^{1}H NMR spectroscopy. In situ reduction of TTC with ASC in basic media produced TF nanoparticles stabilized by the amphiphilic aromatic polymers showing hydrodynamic diameters in the range 100−400 nm, with low size polydispersity and zeta potential in the range −35 to −70 mV. The nanoparticles can be reversibly turned into macro-precipitates upon changing pH. The hypothesis that the amphiphilia of the polyelectrolytes enhances the stabilization of TF nanoparticles synthesized by the method shown here, so that amphiphilic copolymers showing low linear aromatic density and low linear charge density may produce responsive nanoparticles, in contrast to hydrophilic copolymers showing low linear aromatic density and high linear charge density, has been corroborated. Applications of these nanoparticles may stand on the redox properties of the TTC/TF couple, accompanied by color change, as well as on their sensitivity to the pH.

AUTHOR INFORMATION

Corresponding Author

*E-mail: imorenovilloslada@uach.cl.

ORCID

Francesco Picchioni: 0000-0002-8232-2083

Ignacio Moreno-Villoslada: 0000-0003-4125-1220

Notes

The authors declare no competing financial interest.

ACKNOWLEDGMENTS

This work was supported by FONDECYT Regular No. 1050899 and CONICYT-FONDAP 15130011. E.A.-H. thanks CONICYT, Chile, for Doctoral Fellowship No. 72130047.

REFERENCES

(1) Kanazawa, K.; Nakamura, K.; Kobayashi, N. Electroswitchable Optical Device Enabling Both Luminescence and Coloration Control Consisted of Fluoran Dyes and 1,4-Benzoquinone. *Sol. Energy Mater. Sol. Cells* **2016**, *145*, 42−53.

(2) Gingras, M.; Placide, V.; Raimundo, J. M.; Bergamini, G.; Ceroni, P.; Balzani, V. Polysulfurated Pyrene-Cored Dendrimers: Luminescent and Electrochromic Properties. *Chem. - Eur. J.* **2008**, *14*, 10357−10363.

(3) Kanazawa, K.; Nakamura, K.; Kobayashi, N. Electroswitching of Emission and Coloration with Quick Response and High Reversibility in an Electrochemical Cell. *Chem. - Asian J.* **2012**, *7*, 2551−2554.

(4) Nakamura, K.; Kanazawa, K.; Kobayashi, N. Electrochemically-Switchable Emission and Absorption by Using Luminescent Lanthanide(III) Complex and Electrochromic Molecule Toward Novel Display Device with Dual Emissive and Reflective Mode. *Displays* **2013**, *34*, 389−395.

(5) Sagara, Y.; Yamane, S.; Mutai, T.; Araki, K.; Kato, T. A Stimuli-Responsive, Photoluminescent, Anthracene-Based Liquid Crystal: Emission Color Determined by Thermal and Mechanical Processes. *Adv. Funct. Mater.* **2009**, *19*, 1869−1875.

(6) Arimura, T.; Do, J. H.; Tanaka, F. Electrochemically Switchable Molecular-Tweezers. *J. Oleo Sci.* **2017**, *66*, 419−423.

(7) Naumov, P. Photochromism of Ortho-Nitrobenzylpyridines: A Brief Overview. *J. Mol. Struct.* **2006**, *783*, 1−8.

(8) Kishimoto, Y.; Abe, J. A Fast Photochromic Molecule that Colors Only under UV Light. *J. Am. Chem. Soc.* **2009**, *131*, 4227−4229.

(9) Gunnlaugsson, T.; Mac Dónaill, D. A.; Parker, D. Lanthanide Macrocyclic Quinolyl Conjugates as Luminescent Molecular-Level Devices. *J. Am. Chem. Soc.* **2001**, *123*, 12866−12876.

(10) Pino-Pinto, J. P.; Oyarzun-Ampuero, F.; Orellana, S. L.; Flores, M. E.; Nishide, H.; Moreno-Villoslada, I. Aerogels Containing 5,10,15,20-Tetrakis-(4-sulfonatophenyl)-porphyrin with Controlled State of Aggregation. *Dyes Pigm.* **2017**, *139*, 193−200.

(11) Sanhueza, L.; Castro, J.; Urzua, E.; Barrientos, L.; Oyarzun-Ampuero, F.; Pesenti, H.; Shibue, T.; Sugimura, N.; Tomita, W.; Nishide, H.; et al. Photochromic Solid Materials Based on Poly-(decylviologen) Complexed with Alginate and Poly(sodium 4-styrenesulfonate). *J. Phys. Chem. B* **2015**, *119*, 13208−13217.

(12) An, X.; Zhu, A.; Luo, H.; Ke, H.; Chen, H.; Zhao, Y. Rational Design of Multi-Stimuli-Responsive Nanoparticles for Precise Cancer Therapy. *ACS Nano* **2016**, *10*, 5947−5958.

(13) Motornov, M.; Roiter, Y.; Tokarev, I.; Minko, S. Stimuli-Responsive Nanoparticles, Nanogels and Capsules for Integrated Multifunctional Intelligent Systems. *Prog. Polym. Sci.* **2010**, *35*, 174−211.

(14) Babin, J.; Lepage, M.; Zhao, Y. Decoration" of Shell Cross-Linked Reverse Polymer Micelles Using ATRP: A New Route to Stimuli-Responsive Nanoparticles. *Macromolecules* **2008**, *41*, 1246−1253.

(15) Flores, M. E.; Garcés-Jerez, P.; Fernández, D.; Aros-Perez, G.; González-Cabrera, D.; Álvarez, E.; Cañas, I.; Oyarzun-Ampuero, F.; Moreno-Villoslada, I. Facile Formation of Redox-Active Totally Organic Nanoparticles in Water by In Situ Reduction of Organic Precursors Stabilized through Aromatic−Aromatic Interactions by Aromatic Polyelectrolytes. *Macromol. Rapid Commun.* **2016**, *37*, 1729−1734.

(16) Zhang, Y.; Broekhuis, A. A.; Stuart, M. C. A.; Picchioni, F. Polymeric Amines by Chemical Modifications of Alternating Aliphatic Polyketones. *J. Appl. Polym. Sci.* **2008**, *107*, 262−271.

(17) Araya-Hermosilla, R.; Lima, G. M. R.; Raffa, P.; Fortunato, G.; Pucci, A.; Flores, M. E.; Moreno-Villoslada, I.; Broekhuis, A. A.; Picchioni, F. Intrinsic Self-Healing Thermoset Through Covalent and Hydrogen Bonding Interactions. *Eur. Polym. J.* **2016**, *81*, 186−197.

(18) Araya-Hermosilla, R.; Broekhuis, A. A.; Picchioni, F. Reversible Polymer Networks Containing Covalent and Hydrogen Bonding Interactions. *Eur. Polym. J.* **2014**, *50*, 127−134.

(19) Toncelli, C.; Pino-Pinto, J. P.; Sano, N.; Picchioni, F.; Broekhuis, A. A.; Nishide, H.; Moreno-Villoslada, I. Controlling the Aggregation of 5,10,15,20-Tetrakis-(4-sulfonatophenyl)-porphyrin by the Use of Polycations Derived from Polyketones Bearing Charged Aromatic Groups. *Dyes Pigm.* **2013**, *98*, 51−63.

(20) Toncelli, C.; Schoonhoven, M. J.; Broekhuis, A. A.; Picchioni, F. Paal-Knorr Kinetics in Waterborne Polyketone-Based Formulations as Modulating Cross-Linking Tool in Electrodeposition Coatings. *Mater. Des.* **2016**, *108*, 718−724.

(21) Mul, W. P.; Dirkzwager, H.; Broekhuis, A. A.; Heeres, H. J.; van der Linden, A. J.; Orpen, A. G. Highly Active, Recyclable Catalyst for

DOI: 10.1021/acs.jpcb.7b11254
J. Phys. Chem. B 2018, 122, 1747−1755

the Manufacture of Viscous, Low Molecular Weight, CO−Ethene−Propene-Based Polyketone, Base Component for a New Class of Resins. *Inorg. Chim. Acta* **2002**, *327*, 147−159.
(22) Drent, E.; Keijsper, J. J., Polyketone Polymer Preparation with Tetra Alkyl bis Phosphine Ligand and Hydrogen. U.S. Patent 5225523 A, July 6, 1993.
(23) Polgar, L. M.; Lentzakis, H.; Collias, D.; Snijkers, F.; Lee, S.; Chang, T.; Sakellariou, G.; Wever, D. A. Z.; Toncelli, C.; Broekhuis, A. A.; Picchioni, F.; Gotsis, A. D.; Vlassopoulos, D. Synthesis and Linear Viscoelasticity of Polystyrene Stars with a Polyketone Core. *Macromolecules* **2015**, *48*, 6662−6671.
(24) Toncelli, C.; Haijer, A.; Alberts, F.; Broekhuis, A. A.; Picchioni, F. The Green Route from Carbon Monoxide Fixation to Functional Polyamines: a Class of High-Performing Metal Ion Scavengers. *Ind. Eng. Chem. Res.* **2015**, *54*, 9450−9457.
(25) Moreno-Villoslada, I.; González, F.; Rivera, L.; Hess, S.; Rivas, B. L.; Shibue, T.; Nishide, H. Aromatic-Aromatic Interaction between 2,3,5-Triphenyl-2H-tetrazolium Chloride and Poly(sodium 4-styrenesulfonate). *J. Phys. Chem. B* **2007**, *111*, 6146−6150.
(26) Moreno-Villoslada, I.; Torres, C.; González, F.; Soto, M.; Nishide, H. Stacking of 2,3,5-Triphenyl-2H-tetrazolium Chloride onto Polyelectrolytes Containing 4-Styrenesulfonate Groups. *J. Phys. Chem. B* **2008**, *112*, 11244−11249.
(27) Moreno-Villoslada, I.; Jofré, M.; Miranda, V.; Chandía, P.; González, R.; Hess, S.; Rivas, B. L.; Elvira, C.; San Román, J.; Shibue, T.; et al. π-Stacking of Rhodamine B onto Water-Soluble Polymers Containing Aromatic Groups. *Polymer* **2006**, *47*, 6496−6500.
(28) Moreno-Villoslada, I.; González, R.; Hess, S.; Rivas, B. L.; Shibue, T.; Nishide, H. Complex Formation between Rhodamine B and Poly(sodium 4-styrenesulfonate) Studied by ^{1}H-NMR. *J. Phys. Chem. B* **2006**, *110*, 21576−21581.
(29) Waters, M. L. Aromatic Interactions in Model Systems. *Curr. Opin. Chem. Biol.* **2002**, *6*, 736−741.
(30) McGaughey, G. B.; Gagné, M.; Rappé, A. K. π-Stacking Interactions. Alive and Well in Proteins. *J. Biol. Chem.* **1998**, *273*, 15458−15463.
(31) Ikkanda, B. A.; Iverson, B. L. Exploiting the Interactions of Aromatic Units for Folding and Assembly in Aqueous Environments. *Chem. Commun.* **2016**, *52*, 7752−7759.
(32) Lahiri, S.; Thompson, J. L.; Moore, J. S. Solvophobically Driven pi-Staking of Phenylene Ethynylene Macrocycles and Oligomers. *J. Am. Chem. Soc.* **2000**, *122*, 11315−11319.
(33) Cooper, V. R.; Thonhauser, T.; Puzder, A.; Schröder, E.; Lundqvist, B.; Langreth, D. C. Stacking Interactions and the Twist of DNA. *J. Am. Chem. Soc.* **2008**, *130*, 1304−1308.
(34) Yakovchuk, P.; Protozanova, E.; Frank-Kamenetskii, M. D. Base-Stacking and Base-Pairing Contributions into Thermal Stability of the DNA Double Helix. *Nucleic Acids Res.* **2006**, *34*, 564−574.
(35) Tewari, A. K.; Dubey, R. Emerging Trends in Molecular Recognition: Utility of Weak Aromatic Interactions. *Bioorg. Med. Chem.* **2008**, *16*, 126−143.
(36) Waters, M. L. Aromatic Interactions in Peptides: Impact on Structure and Function. *Biopolymers* **2004**, *76*, 435−45.
(37) Versées, W.; Loverix, S.; Vandemeulebroucke, A.; Geerlings, P.; Steyaert, J. Leaving Group Activation by Aromatic Stacking: An Alternative to General Acid Catalysis. *J. Mol. Biol.* **2004**, *338*, 1−6.
(38) Meyer, E. A.; Castellano, R. K.; Diederich, F. Interactions with Aromatic Rings in Chemical and Biological Recognition. *Angew. Chem., Int. Ed.* **2003**, *42*, 1210−1250.
(39) Moreno-Villoslada, I.; Miranda, V.; Gutiérrez, R.; Hess, S.; Muñoz, C.; Rivas, B. L. Interactions of 2,3,5-Triphenyl-2H-tetrazolium Chloride with Poly(sodium 4-styrenesulfonate) Studied by Diafiltration and UV−vis Spectroscopy. *J. Membr. Sci.* **2004**, *244*, 205−213.
(40) Moreno-Villoslada, I.; Soto, M.; González, F.; Montero-Silva, F.; Hess, S.; Takemura, I.; Oyaizu, K.; Nishide, H. Reduction of 2,3,5-Triphenyl-2H-tetrazolium Chloride in the Presence of Polyelectrolytes Containing 4-Styrenesulfonate Moieties. *J. Phys. Chem. B* **2008**, *112*, 5350−5354.
(41) Moreno-Villoslada, I.; Fuenzalida, J. P.; Tripailaf, G.; Araya-Hermosilla, R.; Pizarro, G. C.; Marambio, O. G.; Nishide, H. Comparative Study of the Self-Aggregation of Rhodamine 6G in the Presence of Poly(sodium 4-styrenesulfonate), Poly(N-phenylmaleimide-co-acrylic acid), Poly(styrene-alt-maleic acid), and Poly(sodium acrylate). *J. Phys. Chem. B* **2010**, *114*, 11983−11992.
(42) Moreno-Villoslada, I.; González, F.; Arias, L.; Villatoro, J. M.; Ugarte, R.; Hess, S.; Nishide, H. Control of CI Basic Violet 10 aggregation in aqueous solution by the use of poly (sodium 4-styrenesulfonate). *Dyes Pigm.* **2009**, *82*, 401−408.
(43) Moreno-Villoslada, I.; Flores, M. E.; Marambio, O. G.; Pizarro, G. d. C.; Nishide, H. Polyaromatic-anion behavior of different polyelectrolytes containing benzenecarboxylate units. *J. Phys. Chem. B* **2010**, *114*, 7753−7759.
(44) Araya-Hermosilla, R.; Araya-Hermosilla, E.; Torres-Gallegos, C.; Alarcón-Alarcón, C.; Moreno-Villoslada, I. Sensing Cu 2+ by controlling the aggregation properties of the fluorescent dye rhodamine 6G with the aid of polyelectrolytes bearing different linear aromatic density. *React. Funct. Polym.* **2013**, *73*, 1455−1463.
(45) Moreno-Villoslada, I.; Torres-Gallegos, C.; Araya-Hermosilla, R.; Nishide, H. Influence of the linear aromatic density on methylene blue aggregation around polyanions containing sulfonate groups. *J. Phys. Chem. B* **2010**, *114*, 4151−4158.
(46) Sabaeifard, S.; Abdi-Ali, A.; Soudi, M. R.; Dinarvand, R. Optimization of Tetrazolium Salt Assay for Pseudomonas Aeruginosa Biofilm Using Microtiter Plate Method. *J. Microbiol. Methods* **2014**, *105*, 134−140.
(47) Strlič, M.; Pihlar, B. Determination of Reducing Carbonyl Groups in Cellulose in the Solvent System LiCl/N,N-Dimethylacetamide. *Fresenius' J. Anal. Chem.* **1997**, *357*, 670−675.
(48) Otero, A. J.; Rodríguez, I.; Falero, G. 2, 3, 5−Triphenyi Tetrazolium Chloride (TTC) Reduction as Exponential Growth Phase Marker for Mammalian Cells in Culture and for Myeloma Hybridization Experiments. *Cytotechnology* **1991**, *6*, 137−142.
(49) Nagaraja, P.; Kumar, M. S. H.; Yathirajan, H. S. Silver-Enhanced Reduction of 2,3,5-Triphenyl-2H-Tetrazolium by Semicarbazide for the Spectrophotometric Determination of Traces of Silver I. *Anal. Sci.* **2002**, *18*, 815−817.

DOI: 10.1021/acs.jpcb.7b11254
J. Phys. Chem. B 2018, 122, 1747−1755